

Soft symmetry selection rules in photoemission spectroscopy: The (1×2) phase of hydrogen adsorbed on Ni(110)

Uwe Birkenheuer^{a)}

Lehrstuhl für Theoretische Chemie, Technische Universität München, 85747 Garching, Germany

(Received 16 November 1998; accepted 15 January 1999)

Based on the idea that systems may very well exhibit continuous changes in symmetry if one focuses on physical quantities such as transition matrix elements, the concept of soft symmetry selection rules for dipole transitions is developed. The high-coverage, low-temperature (1×2) -3H phase of H/Ni(110) is chosen to illustrate the new concept. Photoemission measurements on this adsorption system only reveal a single hydrogen-derived band in variance to the stoichiometry of the adlayer. A special procedure to quantitatively decompose the eigenstates of (1×2) -3H/Ni(110) according to their behavior under $2a/3$ translation along $[001]$ is derived. It is demonstrated that this symmetry transformation, though not a strict symmetry element of the adsorption system, can be drawn upon to rationalize the unexpected experimental observations in the spirit of soft symmetry selection. © 1999 American Institute of Physics. [S0021-9606(99)00315-3]

I. INTRODUCTION

Symmetry is one of the most powerful concepts in quantum chemistry. It is applied in many fields of chemistry and material science.¹⁻³ Symmetry selection rules, for instance, are widely used in almost any kind of spectroscopy. The symmetry of orbitals also plays an important role in bonding mechanisms. Crystal and ligand field theory or the Woodward-Hoffmann rules⁴ for cycloaddition are two prominent examples of how symmetry considerations can enter the rationalization of interaction schemes and reaction paths.

This work focuses on dipole selection rules, though the idea of “soft symmetry” which will be presented here is applicable in many areas of quantum chemistry. Basically, dipole selection rules tell whether a transition from an initial state $|i\rangle$ into a final state $|f\rangle$ can be initiated by absorption of a photon of proper energy or not. The probability for such a process is essentially governed by the corresponding dipole transition matrix element

$$\langle i | \mathbf{E} \mathbf{r} | f \rangle, \quad (1)$$

where \mathbf{E} is the polarization vector of the incoming light. Symmetry can then be exploited, such as to tell if certain transition matrix elements have to vanish just because of the symmetry of the electronic states involved. This kind of selection rule will be referred to as “hard” symmetry selection in the following.

The major question always arising when dealing with hard symmetry selection rules is: “Does the system exhibit the required symmetry or not?” At first glance, this seems to be an easy yes-or-no decision. Closer inspection, however, reveals that the situation is a little bit more subtle. Cancellation of transition matrix elements can very well occur for reasons other than strict symmetry. To illustrate that point let us consider the adsorption system $c(2 \times 4)$ -C₂H₄/Ni(110),

which was investigated by means of angle-resolved ultraviolet photoemission spectroscopy (ARUPS) several years ago.⁵ In this combined experimental and theoretical study, the saturated ethylene monolayer was found to exhibit C_2 symmetry only. Yet, dipole selection rules based on local C_{2v} symmetry could successfully be applied to the adsorption system.⁵ Within a subsequent slab model investigation of the unoccupied electronic structure of C₂H₄/Ni(110)⁶ which was carried out in the framework of density functional theory, the occupied Kohn-Sham orbitals of the adsorption complex became accessible as well. In the one-particle picture adopted here these orbitals essentially represent the initial states of the photoemission process. As an example, the ethylene $2b_{1u}$ -derived orbital is shown in Fig. 1. The C_2 symmetry of the monolayer (with respect to vertical rotation axes through the center of each adsorbate) is clearly discernible as are the deviations from local C_{2v} symmetry. Yet, these deviations are rather small, and it is easily comprehensible that, for example in the case of electron detection along the $C=C$ axis, the contributions to the transition matrix element which arise from each side of the $C=C$ axis cancel to a large extent when polarization of the incoming light perpendicular to the $C=C$ axis is considered, whereas no such cancellation occurs for polarization along the $C=C$ axis. In other words, the $2b_{1u}$ -derived orbital shown in Fig. 1 exhibits even (001) mirror plane symmetry in photoemission within the experimental resolution even though the adsorption system itself does not possess this symmetry at all.

The crucial point about this example is that by focusing on the relevant physical quantities, the transition matrix element here, it is possible and also quite reasonable to speak of a *continuous* change from a symmetric to a nonsymmetric behavior of a system. Of course, this concept is not limited to transition matrix elements. It can easily be applied in many other situations. One such example has recently been presented in the context of chiral molecules.⁷ A continuous symmetry deviation measure for a given symmetry transfor-

^{a)}Electronic mail: birkenheuer@ch.tum.de; Fax: ++49 +89 289-13622.

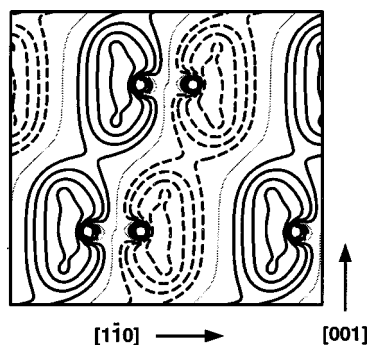


FIG. 1. The ethylene $2b_{1u}$ -derived orbital of the adsorption system $c(2 \times 4)$ - $C_2H_4/Ni(110)$ shown in the (110) plane intersecting the carbon atoms of the adsorbate. The values of the contours are 0.00 (thin line), ± 0.032 , ± 0.056 , ± 0.18 a.u.

mation T has been developed in that study based on the expectation values

$$\chi_i = \langle \psi_i | T | \psi_i \rangle, \quad (2)$$

which were shown to yield a measure for symmetry deviation strictly between 0% (for perfect symmetry) and 100% (for maximum deviation) when summed up properly. Applied to a large variety of molecules, an impressive correlation between this symmetry deviation measure and the experimentally observed amount of chirality was found.⁷

In the same way as symmetry can change continuously from “perfect” over “nearly” down to “not at all,” the vanishing of transition matrix elements due to symmetry can change from “perfect” over “nearly” down to “not at all.” In this sense one might encounter situations where the transition probability of a system is so small that the transition is hardly detectable in experiment anymore. This particular case will be referred to as “soft” symmetry selection in the following; soft in contrast to hard, because we are dealing with threshold arguments here rather than strict yes-or-no decisions as is the case for hard symmetry selection.

There are systems where soft symmetry selection has already been observed in photoemission spectroscopy. The adsorption system $c(2 \times 4)$ - $C_2H_4/Ni(110)$ mentioned above is one of them. Pseudomorphic Cu monolayers on Ni(111) is another example published recently.⁸ Here, a further very interesting but also rather extreme, and thus quite illustrative example, will be presented which has puzzled the experimentalists quite a lot: the low-temperature ($T < 180$ K) high-coverage ($\Theta = 1.5$ ML) phase of hydrogen adsorbed on the Ni(110) surface which exhibits a hydrogen-induced (1×2) pairing row reconstruction. The presentation will mainly focus on the idea of soft symmetry selection rules. Thus after a short introduction to the experimental situation, the symmetry analysis performed will be discussed in detail, followed by a presentation and discussion of the results obtained for the adsorption system (1×2) -3H/Ni(110). Comparison to more recent experimental results is mentioned; yet, the details of that work will be discussed elsewhere.⁹

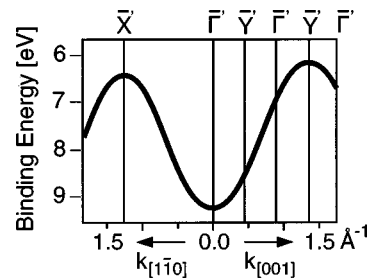


FIG. 2. Schematic view of the hydrogen-induced bands of the adsorption system (1×2) -3H/Ni(110) as obtained by the ARUPS measurements reported in Refs. 10 and 12 (see also Fig. 14 in Ref. 11).

II. EXPERIMENTS

By the time the theoretical investigation on the (1×2) -3H phase of H/Ni(110) presented here was initiated, several independent measurements on the electronic structure of that particular hydrogen phase on Ni(110) had already been performed.^{10–14} In none of them the observed dispersion of the hydrogen-induced bands met the expectations: three occupied hydrogen-induced bands with a periodicity in k -space which reflects the (1×2) surface Brillouin zone of the adsorption system, i.e., which extends 2.52 \AA^{-1} along the Ni rows (the $[1\bar{1}0]$ -direction) and 0.89 \AA^{-1} perpendicular to the Ni rows (the $[001]$ -direction).

The first of these studies, an angle-resolved photoemission investigation on (1×2) -3H/Ni(110) was published by Christmann and co-workers in 1986.^{10,11} Only a single hydrogen-induced band 5–10 eV below the Fermi level was found. Even more surprising: “The H-bands obviously disperse with a triple period along the $[001]$ -direction.”¹⁰ Similar results were obtained a couple of years later by Widdra and co-worker.¹² A schematic sketch of the band structure found in these two studies is given in Fig. 2, a single hydrogen-induced band with a periodicity of 2.68 \AA^{-1} along the $[001]$ -azimuth. In 1987, Komeda *et al.* published another ARUPS measurement on (1×2) -3H/Ni(110).¹³ Likewise, they only found a single H-induced band, dispersing along the Ni rows, but not so along the $[001]$ -direction. However, data were only recorded up to 0.45 \AA^{-1} for the $[001]$ -azimuth and the corresponding photoemission signals in the raw spectra were extremely weak. Therefore any beginning of dispersion in that direction could easily have been overlooked within the limited experimental resolution achieved in this study. The unoccupied states of the adsorption system (1×2) -3H/Ni(110) were investigated as well. In 1990, Bertel and co-worker¹⁴ recorded angle-resolved inverse photoemission spectra and they also found that: “The (1×2) reconstruction is not reflected in the measured dispersion.”¹⁴ Apparently, the hydrogen adlayer behaves more like an unsupported isolated adsorbate layer, at least as far as the periodicity of the electronic surface states is concerned.

To resolve the puzzle of the unexpected periodicity (and number) of hydrogen-derived bands in the adsorption system (1×2) -3H/Ni(110) is one of the main goals of the symmetry analysis presented here.

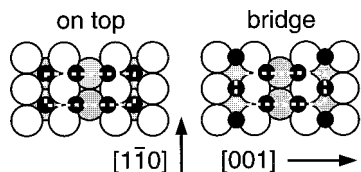


FIG. 3. Two structure models for the adsorption system (1×2) -3H/Ni(110). Hydrogen atoms are displayed in black, subsurface Ni atoms in grey. The (1×2) surface unit cell is indicated as a white box.

III. CALCULATIONS

To investigate the electronic structure of the high-coverage, low-temperature phase of H/Ni(110), density functional repeated slab calculations have been performed. The geometry of the substrate was taken from a LEED (low energy electron diffraction) analysis of the hydrogen-induced reconstruction of (1×2) -3H/Ni(110).¹⁵ The hydrogen positions are not reported in that study. However, in another LEED analysis of the closely related low-temperature (2×1) -2H phase of H/Ni(110),¹⁶ the position of the adsorbed hydrogen atoms could be resolved. They are threefold coordinated to two surface and one subsurface Ni atom each with a H-Ni distance of 1.72 ± 0.01 Å to all three nearest-neighbor Ni atoms and related to each other by glide plane symmetry. An EELS (electron energy loss spectroscopy) analysis¹⁷ further revealed that two of the hydrogen atoms (per unit) in the high-coverage (1×2) -3H/Ni(110) phase are very similar to the threefold coordinated hydrogen atoms in the (2×1) -2H/Ni(110) phase (exhibiting local $C_s [\sigma_{(1\bar{1}0)}]$ symmetry), whereas the third hydrogen atom, a different adsorption species, exhibits local $C_s [\sigma_{(001)}]$ symmetry. Therefore, this third H-atom must either be located directly above the paired Ni rows of the (1×2) -reconstructed Ni(110) surface, or precisely in between these paired rows. For sterical reasons, location of the single hydrogen was assumed above the paired rows. Two idealized structure models were constructed on the base of the experimental data available (Fig. 3), one with all three hydrogen atoms aligned (the on top model), and the other with the single H-atom shifted along $[1\bar{1}0]$ into a bridge position (with respect to the second Ni layer). However, as far as the electronic structure and especially the features of the hydrogen-derived states are concerned, these two structure models yield rather similar results (see Sec. V). Thus, we mainly focus on the on top model of the adsorption system (1×2) -3H/Ni(110) because it is more appropriate for the concept of soft symmetry deviation to be discussed here. Yet, in a Ne atom diffraction study,^{18,19} Rieder and co-worker found the simulated corrugation of the on top model to be less compatible with the ion diffraction results than with their favored structure model, which is similar to the bridge model proposed here except that the two threefold hydrogen atoms are located above the paired rows and the single hydrogen atom in between.^{18,19}

The calculations were performed with the WIEN95 code,²⁰ an implementation of the Kohn-Sham approach to density functional theory within the FLAPW (full potential linearized augmented plane wave) methodology. The gradient-corrected functionals suggested by Perdew and

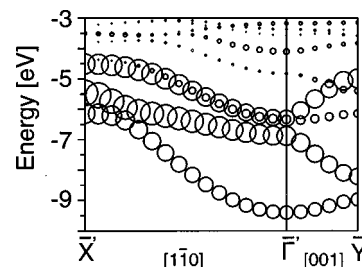


FIG. 4. Minority spin band structure of the on top model for (1×2) -3H/Ni(110) restricted to even states with respect to the central layer mirror plane. The radii of the circles indicate the hydrogen population (see text for details).

Wang in 1991²¹ have been used throughout. All calculations have been carried out spin-polarized. The adsorption system was modeled by slabs of five substrate layers with the lattice constant a set to the experimental bulk value of 3.52 Å,¹⁶ and with hydrogen being adsorbed on both sides of the slabs. For the hydrogen atoms above the paired nickel rows, the nearest-neighbor H-Ni distance found for the threefold coordinated H-atoms, 1.72 Å,¹⁶ was adopted. The individual model slabs were separated by 6.22 Å, which corresponds to the thickness of five substrate layers. Dispersion of the occupied bands perpendicular to the surface was found to be negligible for that setup. Because of the surface reconstruction, the relaxation, and the buckling, the radius of the muffin-tin spheres of Ni had to be chosen rather small, 2.0 bohr. The radius of the hydrogen muffin-tin spheres was set to 0.8 bohr. Despite the presence of such small muffin-tin spheres, the plane wave expansion of the basis functions within the interstitial region was truncated at 16.0 Ry, a typical value for the Ni substrate. For the potential representation, a plane wave cutoff of 100.0 Ry was used. The surface Brillouin zone was sampled by 6×2 k -points, and the k -space integration was carried out by means of the modified tetrahedron method.²²

In Fig. 4 the calculated band structure of the on top model of (1×2) -3H/Ni(110) is shown. The hydrogen population of each Bloch state, here defined as the integrated charge inside the hydrogen muffin-tin spheres, is indicated by the radii of the circles. Three things can be noticed right away: (i) the only hydrogen-dominated feature discernible is the broad resonance at the bottom of the Ni valence band, (ii) this resonance is formed by *three* hydrogen-derived states per k -point, and (iii) the dispersion of these hydrogen bands precisely matches the (1×2) -periodicity of the adsorption system, i.e., 1.34 Å⁻¹ are required to reach the surface Brillouin zone boundary \bar{X}' in the $[1\bar{1}0]$ -direction, but only 0.45 Å⁻¹ to reach the point of return along the $[001]$ -azimuth. The nature of the metallic band crossing the hydrogen resonance between -4.5 and -6.0 eV will be discussed later (Sec. VI).

Actually, only the minority spin band structure is displayed in Fig. 4. Yet, the band structure of the majority spin looks very much the same. The only difference is that the entire Ni d -band (down to about -3.5 eV) is shifted downward by about 0.3 eV, whereas the energy of the hydrogen-derived bands is not altered significantly (deviations < 0.1

eV). This is an often observed feature of magnetic materials such as Ni (e.g., Ref. 23 and references therein). Upon adsorption, the magnetism is totally quenched within the first few surface layers whereas it remains essentially unchanged in the bulk layers below.

Furthermore, in Fig. 4 only the bands of those states are shown which are even with respect to the mirror plane through the central substrate layer of the model slab. This has been done to account for the ‘‘sandwich’’-model adopted. Each surface state exists twice in such a model, once at the upper side and once at the opposite side of the slab. If localized enough, these states will not interfere, i.e., their symmetric and the antisymmetric linear combinations will exhibit essentially the same one-particle energy, and thus doubly degenerated bands will occur. In the present case, the hydrogen-derived states at both sides of the model slab are not perfectly decoupled. The hydrogen-dominated bands of the odd states run essentially parallel to those of the even states with a uniform shift of about 0.2 to 0.5 eV depending on band index and azimuth. Apparently, the hydrogen-derived states are too distended to be separated entirely by five substrate layers. The major results of the following symmetry analysis, however, are not affected by this spurious interaction.

IV. SYMMETRY ANALYSIS

There are definitely *three* hydrogen-derived bands in the band structure of the surface adsorption system (1×2) -3H/Ni(110), and they definitely exhibit a periodicity of 0.89 \AA^{-1} along the [001]-azimuth. Yet, only one hydrogen band is discernible in the experiments, and this single band seems to disperse with a period of 2.68 \AA^{-1} along [001] which would correspond to an effective $(1 \times 2/3)$ overlayer. As will be demonstrated, soft symmetry selection is the reason for that discrepancy.

In view of the specific arrangement of the hydrogen adatoms in the structure models proposed (Fig. 3), a uniform translation of the entire adsorption system by $2a/3$ along the [001]-direction is the most promising candidate in (1×2) -3H/Ni(110) for generating the kind of minor-symmetry-deviation-only effect which is required for soft symmetry selection to occur. In fact, because this particular symmetry transformation is a member of the space group of the effective $(1 \times 2/3)$ overlayer—though it is not a symmetry element of the total adsorption system—it is likely that soft symmetry selection according to this symmetry transformation will produce the experimentally observed effective band structure of the hydrogen adlayer. The remaining part of the section is therefore organized as follows. First it will be shown that by means of the $2a/3$ translation along [001], each Bloch state $\psi_k^{1 \times 2}$ of the (1×2) -periodic adsorption system can uniquely be split into three contributions $\varphi_{k+\nu(\pi/a)}^{1 \times 2/3}$, each of them being a quasiperiodic Bloch function of the effective $(1 \times 2/3)$ overlayer. This splitting is the base for the symmetry analysis of (1×2) -3H/Ni(110). Next, the necessary condition for soft symmetry selection will be discussed, and finally an explicit procedure to check for this condition is presented.

Let us turn to the decomposition of the Bloch state $\psi_k^{1 \times 2}$. Splitting off the phase factor e^{ikr} , each Bloch state $\psi_k^{1 \times 2}$ of the adsorption system can be regarded as a (1×2) -periodic function in space which can easily be expressed by its Fourier series,

$$\psi_k^{1 \times 2}(r) = e^{ikr} \sum_{K \in \mathcal{G}_{1 \times 2}^*} a_K(k) e^{iKr}, \quad (3)$$

with $\mathcal{G}_{1 \times 2}^*$ being the reciprocal lattice of the (1×2) reconstructed surface system. Now, each reciprocal lattice vector K can uniquely be written as a reciprocal lattice vector Q of the effective $(1 \times 2/3)$ overlayer plus an offset vector $q_\nu = \nu \pi/a e_{[001]}$ with $\nu=0,1,2$. The sum over K can therefore be substituted by a double sum over Q and ν , resulting in

$$\psi_k^{1 \times 2}(r) = \sum_{\nu=0}^2 \left\{ e^{i(k+q_\nu)r} \sum_{Q \in \mathcal{G}_{1 \times 2/3}^*} a_{Q+q_\nu}(k) e^{iQr} \right\}. \quad (4)$$

The inner sum over Q in this expression actually defines three different $(1 \times 2/3)$ -periodic functions which together with the prefactor $e^{i(k+q_\nu)r}$ yield the Bloch wave contributions $\varphi_{k+q_\nu}^{1 \times 2/3}$ we are looking for,

$$\psi_k^{1 \times 2}(r) = \sum_{\nu=0}^2 \varphi_{k+\nu \pi/a}^{1 \times 2/3} e_{[001]}. \quad (5)$$

Assuming that the final state of the photoemission process is dominated by the plane wave contribution $e^{ik_{\text{elec}}r}$ where k_{elec} is the wave vector of the out-going electron, each of the contributing Bloch functions $\varphi_{k+q_\nu}^{1 \times 2/3}$ can only add significantly to the photoemission signal, if

$$k_{\text{elec}} = k + \nu \frac{\pi}{a} e_{[001]} + Q. \quad (6)$$

This relation reflects the hard symmetry selection rule for the individual Bloch function contributions $\varphi_{k+q_\nu}^{1 \times 2/3}$. We now come to the crucial point of the symmetry analysis. If for a given crystal momentum k , for some reason an initial Bloch state $\psi_k^{1 \times 2}$ essentially coincides with just *one* of its contributions $\varphi_{k+q_\nu}^{1 \times 2/3}$,

$$\psi_k^{1 \times 2} \approx \varphi_{k+q_{\nu(k)}}^{1 \times 2/3}, \quad (7)$$

a noticeable transition probability can only occur if condition (6) holds for the specific $\nu(k)$. Thus substituting ν by $\nu(k)$ Eq. (6) also describes the *soft* symmetry selection rule for the adsorption system (1×2) -3H/Ni(110). Since Q is a reciprocal lattice vector of the effective $(1 \times 2/3)$ overlayer, a periodicity of 2.68 \AA^{-1} along the [001]-azimuth is automatically generated by this soft selection rule. However, because the crystal momentum along [001] just varies between -0.45 and $+0.45 \text{ \AA}^{-1}$, only partially visible bands within the extended Brillouin zone of the effective overlayer can arise from the soft selection condition (6). We will return to that point in the next section.

Assumption (7) is the key for soft symmetry selection to occur in (1×2) -3H/Ni(110). To check for this assumption to hold, and to quantify the amount of coincidence, the following three k -dependent projectors,

$$P_k^\nu[\psi](r) = \frac{1}{3} \sum_{j=0}^2 e^{i(kt + 2\pi/3\nu)j} \psi(r - jt), \quad (8)$$

with $t = 2a/3 e_{[001]}$, are defined in close analogy to the projectors used in group theory to generate basis functions for the individual irreducible representations of a group.²⁴ It can easily be shown (see Appendix) that when the P_k^ν act on the subspace of Bloch states with crystal momentum k , the following two relations,

$$\sum_{\nu=0}^2 P_k^\nu = 1 \quad \text{and} \quad P_k^\nu P_k^\mu = \delta_{\nu\mu} P_k^\nu, \quad (9)$$

hold, and that the images of P_k^ν are indeed Bloch functions of the effective $(1 \times 2/3)$ overlayer with crystal momentum $k + q_\nu$. Because of these completeness and orthogonality relations of the projectors P_k^ν , the individual $\varphi_{k+q_\nu}^{(1 \times 2/3)}$ contributions of a Bloch state $\psi_k^{(1 \times 2)}$ can simply be obtained by projection,

$$\varphi_{k+q_\nu}^{(1 \times 2/3)} = P_k^\nu[\psi_k^{(1 \times 2)}]. \quad (10)$$

In addition, their squared norms

$$\chi_k^\nu = |\varphi_{k+q_\nu}^{(1 \times 2/3)}|^2 \quad (11)$$

can be expressed as simple expectation values,

$$\chi_k^\nu = \langle \psi_k^{(1 \times 2)} | P_k^\nu | \psi_k^{(1 \times 2)} \rangle, \quad (12)$$

and the following sum rule holds:

$$\chi_k^\nu \in [0, 1] \quad \text{with} \quad \sum_{\nu=0}^2 \chi_k^\nu = 1. \quad (13)$$

Because of Eq. (13), the quantities χ_k^ν introduced here are perfectly suited as a measure for the amount of the individual $\varphi_{k+q_\nu}^{(1 \times 2/3)}$ contributions. This measure ranges from 0% (for no admixture at all) up to 100% (for ultimate coincidence). Therefore, the determination of expectation values of symmetry projectors such as P_k^ν [see Eq. (12)] has been implemented in the WIEN95 code.²⁵ For simplicity, the evaluation is not performed on the real eigenfunctions ψ_{nk} but on the pseudo orbitals, i.e., those orbitals which result when the Fourier expansion of ψ_{nk} within the interstitial region is extrapolated into the muffin-tin spheres. It is believed, however, that this approximation does not influence the overall qualitative picture drawn from the symmetry analysis presented here (see next section).

V. RESULTS

The symmetry analysis suggested in the previous section has been applied to both the on top and the bridge model of the adsorption system (1×2) -3H/Ni(110). In Fig. 5 the expectation values χ_k^ν obtained for the on top model are shown. Note, that here the radii of the circles indicate the individual admixture of the Bloch wave contributions $\varphi_{k+q_\nu}^{(1 \times 2/3)}$ rather than the hydrogen population. Instead, the hydrogen-dominated bands are marked bold. Let us consider the $[001]$ -azimuth first. Clearly, each of the three hydrogen bands is dominated by a single Bloch wave contribution, the lowest

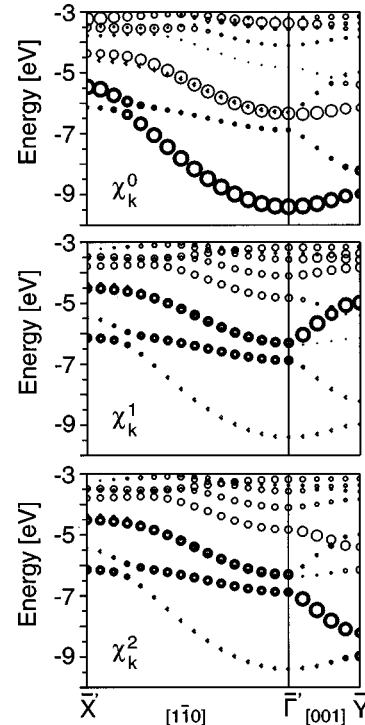


FIG. 5. Decomposition of the minority spin band structure of the even states of the on top model for (1×2) -3H/Ni(110) into Bloch wave contributions of the effective $(1 \times 2/3)$ overlayer. The radii of the circle are proportional to the respective contribution measures χ_k^ν ($\nu=0,1,2$) derived in Sec. IV. The hydrogen-dominated bands are displayed in bold.

band by the “ $\nu=0$ ”-contribution, the second band by the “ $\nu=2$ ”-contribution and the highest band by the “ $\nu=1$ ”-contribution. Thus, beyond any doubt, the condition for soft symmetry selection is fulfilled.

Somewhat surprising, at first glance, is the sudden breakdown of the dominance of the respective Bloch wave contribution at the high symmetry points $\bar{\Gamma}'$ and \bar{Y}' (Fig. 5). This can, however, easily be explained. The (001) mirror plane σ is a symmetry operation for both high symmetry points along $[001]$. Therefore, with $D(\sigma)$ as the corresponding symmetry operator, $D(\sigma)[\psi_k^{(1 \times 2)}] = \pm \psi_k^{(1 \times 2)}$ for any Bloch state $\psi_k^{(1 \times 2)}$ at $\bar{\Gamma}'$ or \bar{Y}' . As a consequence,

$$\chi_k^\nu = \langle \psi_k^{(1 \times 2)} | D(\sigma^{-1}) P_k^\nu D(\sigma) | \psi_k^{(1 \times 2)} \rangle \quad \text{with} \quad (14)$$

$$D(\sigma^{-1}) P_k^\nu D(\sigma) = P_{-k}^{(-\nu) \bmod 3} = P_{\pi/a e_{[001]} - k}^{(-\nu-1) \bmod 3}. \quad (15)$$

The proof is straightforward. From Eq. (15) it immediately follows that at the $\bar{\Gamma}'$ -point $P_{\bar{\Gamma}'}^1 = P_{\bar{\Gamma}'}^2$, and thus the Bloch wave contributions for $\nu=1$ and $\nu=2$ must be equal. Similarly, at the \bar{Y}' -point Eq. (15) yields $P_{\bar{Y}'}^0 = P_{\bar{Y}'}^2$, so that here the “ $\nu=0$ ” and “ $\nu=2$ ” Bloch wave contributions must be equal. Both are confirmed by Fig. 5.

Essentially the same arguments hold for the $[1\bar{1}0]$ -azimuth. Here the (001) mirror plane is a symmetry element for all k -points on the high symmetry line between \bar{X}' and $\bar{\Gamma}'$. Thus equal “ $\nu > 0$ ” Bloch wave contributions have to occur along the entire $[1\bar{1}0]$ -direction (Fig. 5). This degeneracy, however, does not affect the most important feature of

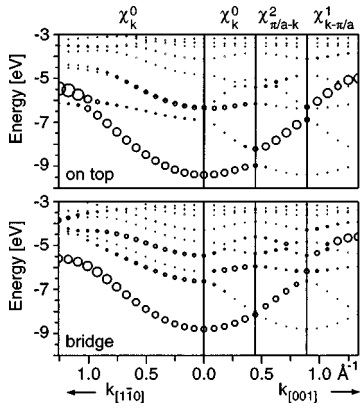


FIG. 6. Minor spin band structure of the even states of the on top (upper panel) and the bridge model (lower panel) of (1×2) -3H/Ni(110) weighted by the hydrogen population and the Bloch wave contribution measure χ_k^ν as indicated to simulate the soft symmetry selection occurring in that adsorption system.

the symmetry analysis in the present context: Evidently, the lowest hydrogen band is strongly dominated by its $\varphi_{k+q_0}^{(1 \times 2/3)}$ contribution, whereas the other two hydrogen bands only exhibit minor “ $\nu=0$ ”-admixture.

Thus the puzzle of the hydrogen-derived bands in (1×2) -3H/Ni(110) is essentially solved. We only have to put the pieces together. For electron detection along the $[1\bar{1}0]$ -direction the soft symmetry selection rule (6) can only be fulfilled for $\nu=0$. Hence only the lowest hydrogen-dominated band is observable in photoemission spectra recorded for $[1\bar{1}0]$ -azimuth. The other two bands most probably stay hidden in the background intensity. In case of electron detection along the $[001]$ -direction, the situation is a little bit more complicated. As already mentioned, the relevant crystal momentum $k_{[001]}$ only varies between 0.0 and 0.45 \AA^{-1} (see Fig. 5). Hence for electron wave vectors $k_{[001]}^{\text{elec}}$ between 0.0 and 0.45 \AA^{-1} (0 and $\pi/2a$), the “ $\nu=0$ ” channel is selected by the symmetry condition (6), whereas for electron wave vectors between 0.89 and 1.34 \AA^{-1} (π/a and $3\pi/2a$) the “ $\nu=1$ ” channel is selected, i.e.,

$$k_{[001]}^{\text{elec}} = k_{[001]} + \frac{\pi}{a} \quad \text{with} \quad k_{[001]} \in \left[0, \frac{\pi}{2a}\right]. \quad (16)$$

For electron wave vectors between 0.45 and 0.89 \AA^{-1} , or equivalently wave vectors $-k^{\text{elec}}$ between -0.89 and -0.45 \AA^{-1} , finally,

$$-k_{[001]}^{\text{elec}} = k_{[001]} - \frac{\pi}{a} = \left(k_{[001]} + \frac{2\pi}{a}\right) \text{mod } \mathcal{G}_{1 \times 2/3}^*, \quad (17)$$

and thus the “ $\nu=2$ ”-contributions are selected in that case.

These considerations are summarized in Fig. 6, where the band structure of the adsorption system is depicted as a function of the electron momentum k^{elec} . To incorporate the soft symmetry selection rules just explained, the hydrogen populations are weighted by the appropriate Bloch wave contribution measure in each panel of the repeated zone scheme, i.e., by $\chi_{k^{\text{elec}}}^0$ in the first panel of both azimuths, by $\chi_{\pi/a - k^{\text{elec}}}^2$ in the second panel along $[001]$, and by $\chi_{k^{\text{elec}} - \pi/a}^1$ in the third panel along $[001]$. For comparison, the results for

the bridge model are given as well. Due to soft symmetry selection only a single hydrogen-induced feature remains, which within limited experimental resolution seems to be a single band exhibiting a periodicity of 2.68 \AA^{-1} along the $[001]$ -direction. Essentially the same result is found for the bridge model, though the adsorbed hydrogen atoms are no longer aligned in this structure and only minor symmetry deviation with respect to a $2a/3$ translation along $[001]$ is not that easy to comprehend.

An interesting difference between the on top and the bridge model is the different amount of band splitting found at the first \bar{Y}' -point. Closer inspection, however, reveals that this feature is very sensitive to the coupling of the top and bottom adlayers of the “sandwich”-models. Quite a different splitting was found for the hydrogen-dominated bands arising from the *odd* eigenstates of the slab models. Much thicker substrate slabs would be required to achieve model convergence for that special feature.

VI. DISCUSSION

In the previous section it has been demonstrated how soft symmetry selection results in a single hydrogen-induced band in the photoemission spectra of (1×2) -3H/Ni(110). Yet, soft symmetry selection is a threshold effect, and by enhanced experimental effort it should, at least in principle, be possible to resolve all three hydrogen bands. This has, in fact, been demonstrated very impressively in a new and very recent reinvestigation of the electronic structure of (1×2) -3H/Ni(110) by means of angle-resolved photoemission spectroscopy.⁹ In this study it was possible to observe *all* three hydrogen-induced features, two of them expectedly weak, and band dispersions precisely as shown in Fig. 4 are found.

Yet, two questions remain. What is the nature of the metallic band crossing the hydrogen resonance at about -5 eV, and how can the occurrence of soft symmetry selection be understood? To answer these questions, the possibility of visualizing crystal orbitals has been implemented in the WIEN95 code.²⁵ Focusing again on the on top structure, the four lowest valence crystal orbitals at the $\bar{\Gamma}'$ -point are shown in Fig. 7 for the on top model of the adsorption system (1×2) -3H/Ni(110).

The lowest state at $\bar{\Gamma}'$, the $\bar{\Gamma}'_1$ state, is localized to a large extent on the hydrogen atoms, and thus exhibits the typical behavior of a surface state which energetically falls below the valence band of the substrate. Within the hydrogen adlayer, invariance of the crystal orbital with respect to a $2a/3$ translation along the $[001]$ -direction is easy to comprehend (see Fig. 7). This pseudosymmetry is only locally destroyed by the presence of the substrate atoms and the necessity for orthogonality onto the Ni core orbitals. According to the symmetry analysis of the second and third hydrogen-related features, the $\bar{\Gamma}'_2$ and $\bar{\Gamma}'_4$ orbitals should be dominated in equal parts by Bloch waves $\varphi^{(1 \times 2/3)}$ with crystal momentum $\pm \pi/a e_{[001]}$, or more precisely by the corresponding sine and cosine linear combinations, because the orbitals at the $\bar{\Gamma}'$ -point have to be real functions. Inspection of Fig. 7 confirms that these orbitals indeed exhibit as best as possible

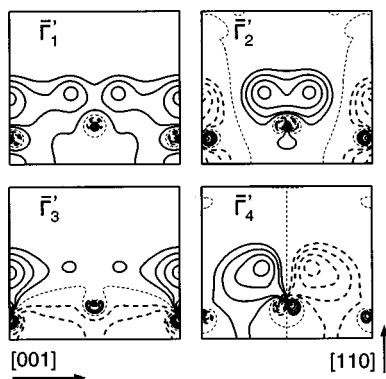


FIG. 7. The four lowest minor spin valence orbitals at Γ' of the on top model of the adsorption system (1×2) -3H/Ni(110) displayed in the $(1\bar{1}0)$ plane intersecting the adsorbed hydrogen atoms. The values of the contour lines are 0.00 (short dashed line), ± 0.025 , ± 0.040 , ± 0.063 , ± 0.10 , and ± 0.16 a.u.

the typical shape of a sine and cosine wave with a wavelength of π/a . At least it is evident from Fig. 7 why transition matrix elements with final state wave functions describing, say, electrons in normal emission essentially vanish for light polarization along the surface normal. In contrast to the Γ'_1 state, which is a typical surface state, the energetically higher lying hydrogen states resemble surface resonances, states which thus propagate into the bulk but still exhibit enhanced wave function amplitudes at the surface. This finding is in line with the fact that the energy of these particular hydrogen-derived states falls *into* the valence band of the Ni substrate.

The remaining orbital, Γ'_3 , represents the metallic band crossing the hydrogen resonance. As is revealed by Fig. 7, this state actually is a bulk Bloch wave which is “scattered back” at the surface state Γ'_1 , i.e., which has to be orthogonal to the latter one and thus contains a nodal plane parallel to the surface and close to the hydrogen adlayer. Yet, the significant participation of the on top hydrogen atom is somewhat unexpected for such a “scattering state.” This feature is probably related to the close energetic proximity to the Γ'_4 state that for symmetry reasons cannot contain any orbital admixture from the on top hydrogen atom at all. Nevertheless, the Γ'_3 orbital clearly exhibits the highest substrate participation and the lowest hydrogen population among the four valence orbitals discussed here. Qualitatively similar figures are obtained for the \bar{Y}' -point as well as for the bridge model.

VII. SUMMARY

Density functional slab model calculations have been performed for two different structure models of the high-coverage, low-temperature (1×2) -3H phase of H/Ni(110). It could be shown that upon hydrogen chemisorption a broad resonance at the bottom of the Ni valence band is formed which consists of *three* individual hydrogen-dominated states per k -point whose energy bands disperse precisely according to the (1×2) -periodicity of the entire adsorption system. Nevertheless, only a single hydrogen-derived band

which exhibits the dispersion of an effective $(1 \times 2/3)$ overlayer could be observed in various photoemission experiments.^{10–14} To resolve this puzzle, the concept of soft symmetry selection was derived and adapted to the specific situation of the pseudo $2a/3$ translation symmetry along the $[001]$ -direction encountered in the adsorption system (1×2) -3H/Ni(110). To this end, three orthogonal projectors P_k^ν ($\nu=0,1,2$) were defined which allowed a *quantitative* decomposition of each Bloch state into Bloch waves of the effective $(1 \times 2/3)$ overlayer. Applied to the hydrogen-dominated states of the adsorption system, this procedure clearly revealed that the condition for soft symmetry selection is fulfilled, i.e., that each of the corresponding eigenstates of (1×2) -3H/Ni(110) is dominated by a *single* Bloch wave contribution of the effective overlayer. Combining soft symmetry selection and surface sensitivity (see Fig. 6), a band structure with a single hydrogen-dominated state per k -point could be derived. Within limited experimental resolution this state seemingly exhibits $(1 \times 2/3)$ dispersion along the $[001]$ -azimuth as observed experimentally. Very recent ARUPS measurements⁹ confirm the existence of two further, but rather weak emitting hydrogen-derived bands in (1×2) -3H/Ni(110). In summary, the adsorption system (1×2) -3H/Ni(110) provides a very nice example of how minor-symmetry-deviation effects such as the soft symmetry selection rule discussed here can successfully be applied in quantum chemistry or surface science to rationalize features which at first glance seem to be in variance with the overall symmetry of the system under study.

ACKNOWLEDGMENTS

I thank W. Widdra for bringing the 3H/Ni(110) surface system to my attention and for providing the results of his experiments before publication. Furthermore, I am thankful for the many discussions with W. Widdra and M. Lindroos. Personal and financial support from N. Rösch and the Deutsche Forschungsgemeinschaft via SFB 338 is also gratefully acknowledged.

APPENDIX: SYMMETRY PROJECTORS

In a slight generalization of the situation encountered in Sec. IV, the following general statement will be proven rigorously:

“Let G be a two-dimensional lattice with primitive lattice vectors a_1 and a_2 and $t = a_2/N$ an integer fraction of a_2 , then the operators

$$P_k^\nu[\psi](r) = \frac{1}{N} \sum_{j=0}^{N-1} e^{i(k t + 2\pi/N \nu) j} \psi(r - j t) \quad (\text{A1})$$

form a set of mutual orthogonal projectors when acting on the subspace of Bloch functions with momentum k which sum up to identity and whose images yield Bloch function of the $(1 \times 1/N)$ sublattice with momentum $k + \nu b_2$ each, where b_1 and b_2 are the reciprocal basis vectors of the lattice basis $\{a_1, a_2\}$, i.e., $a_i \cdot b_j = 2\pi \delta_{ij}$.”

Let us first introduce the short-hand notation $\varphi_k^\nu = P_k^\nu[\psi_k]$. A $1/N$ translation t along a_2 applied to such a function results in

$$\begin{aligned}\varphi_k^v(r-t) &= \frac{1}{N} \sum_{j=0}^{N-1} e^{i(kt+2\pi/N)vj} \psi_k(r-(j+1)t) \\ &= e^{-i(kt+2\pi/N)v} \left\{ \frac{1}{N} \sum_{j=1}^N e^{i(kt+2\pi/N)vj} \psi_k(r-jt) \right\}.\end{aligned}\quad (\text{A2})$$

$$\quad (\text{A3})$$

Since $t \cdot N = a_2$, the “ $j=N$ ”-term of the inner sum in Eq. (A3) actually reads

$$e^{i(ka_2+2\pi v)} \psi_k(r-a_2), \quad (\text{A4})$$

which is equal to the “ $j=0$ ”-term, $\psi_k(r)$, because v is an integer, a_2 a lattice vector, and ψ_k a Bloch function of the lattice G . The sum from $j=1$ to N can therefore be replaced by a sum running from $j=0$ to $N-1$ resulting in

$$\varphi_k^v(r-t) = e^{-i(kt+2\pi/N)v} \varphi_k^v(r). \quad (\text{A5})$$

Using $t \cdot b_2 = a_2 \cdot b_2 / N = 2\pi/N$, the effect of a translation operation on the functions ψ_k^v can also be expressed as

$$\varphi_k^v(r-t) = e^{-i(k+vb_2)t} \varphi_k^v(r). \quad (\text{A6})$$

Similarly,

$$\varphi_k^v(r-a_1) = \frac{1}{N} \sum_{j=0}^{N-1} e^{i(kt+2\pi/N)vj} \psi_k(r-jt-a_1) \quad (\text{A7})$$

$$= e^{-ika_1} \psi_k(r), \quad (\text{A8})$$

because a_1 is a lattice vector and ψ_k a Bloch function. Taking advantage of $a_1 \cdot b_2 = 0$, Eq. (A8) can be cast into the same form as Eq. (A6),

$$\varphi_k^v(r-a_1) = e^{-i(k+vb_2)a_1} \varphi_k^v(r). \quad (\text{A9})$$

Together these two equations tell that for any Bloch state ψ_k the image function $\varphi_k^v = P_k^v[\psi_k]$ is a Bloch function of the effective $(1 \times 1/N)$ overlayer with momentum $k + vb_2$.

Next, consider the completeness relation $\sum_{\nu=0}^{N-1} P_k^\nu = 1$. Applying the definition (A1) and rearranging the order of the summation yields

$$\sum_{\nu=0}^{N-1} P_k^\nu[\psi](r) = \frac{1}{N} \sum_{j=0}^{N-1} e^{-iktj} \left\{ \sum_{\nu=0}^{N-1} (e^{-i2\pi/Nj})^\nu \right\} \psi(r-jt). \quad (\text{A10})$$

Because

$$\sum_{\nu=0}^{N-1} q^\nu = \begin{cases} (1-q^N)/(1-q) & \text{if } q \neq 1 \\ N & \text{else} \end{cases}, \quad (\text{A11})$$

the sum within the braces in Eq. (A10) reduces to $N \delta_{j0}$ and thus

$$\sum_{\nu=0}^{N-1} P_k^\nu[\psi](r) = \psi(r) \quad (\text{A12})$$

for any function ψ .

Finally, the orthogonality relation has to be proven. Using definition (A1) and applying the index transformation $l \rightarrow l+j$ results in

$$\begin{aligned}P_k^\nu P_k^\mu[\psi_k](r) &= \frac{1}{N^2} \sum_{j,l=0}^{N-1} e^{i(kt+2\pi/N)vj} e^{i(kt+2\pi/N\mu)l} \psi_k(r-jt-lt) \\ &= \frac{1}{N^2} \sum_{j=0}^{N-1} e^{i2\pi/N(\nu-\mu)j} \sum_{l=j}^{N+j-1} e^{i(kt+2\pi/N\mu)l} \psi_k(r-lt).\end{aligned}\quad (\text{A13})$$

$$\quad (\text{A14})$$

By the same arguments already used to transform the “ $j=N$ ”-term in Eq. (A3) into the “ $j=0$ ”-term, the inner sum over l can be reexpressed as a sum running from 0 to $N-1$. After this transformation, the summation over j only acts on the exponential prefactor, and therefore [after applying Eq. (A11) again] reduces to $N \delta_{\nu\mu}$. Hence

$$P_k^\nu P_k^\mu[\psi_k](r) = \delta_{\nu\mu} \frac{1}{N} \sum_{l=0}^{N-1} e^{i(kt+2\pi/N\mu)l} \psi_k(r-lt) \quad (\text{A15})$$

$$= \delta_{\nu\mu} P_k^\mu[\psi_k](r). \quad (\text{A16})$$

¹T. A. Albright, J. K. Burdett, and M.-H. Whangbo, *Orbital Interaction in Chemistry* (Wiley, New York, 1985).

²P. W. Atkins, *Physical Chemistry* (Oxford University Press, New York, 1986).

³F. A. Cotton, *Chemical Applications of Group Theory* (Wiley, New York, 1990).

⁴R. B. Woodward and R. Hoffmann, *Angew. Chem.* **81**, 797 (1969).

⁵M. Weinelt, W. Huber, P. Zebisch, H.-P. Steinrück, B. Reichert, U. Birkenheuer, and N. Rösch, *Phys. Rev. B* **46**, 1675 (1992).

⁶U. Gutdeutsch, U. Birkenheuer, E. Bertel, J. Cramer, J. C. Boettger, and N. Rösch, *Surf. Sci.* **345**, 331 (1996).

⁷S. Grimme, *Chem. Phys. Lett.* **297**, 15 (1998).

⁸H. Koschel, G. Held, P. Trischberger, W. Widdra, U. Birkenheuer, and H.-P. Steinrück, *Appl. Surf. Sci.* (in press).

⁹W. Widdra, in preparation.

¹⁰K. Christmann, M. Ehsasi, K. H. Ernst, H. Kühlenbeck, N. Neumann, H. Saalfeld, and E. Schwarz, *BESSY Jahresbericht 1986*, p. 206.

¹¹K. Christmann, *Surf. Sci. Rep.* **9**, 1 (1988).

¹²W. Widdra (private communication).

¹³T. Komeda, Y. Sakisaka, M. Onchi, H. Kato, S. Masuda, and K. Yagi, *Phys. Rev. B* **36**, 922 (1987).

¹⁴G. Rangelow, N. Memmel, E. Bertel, and V. Dose, *Surf. Sci.* **236**, 250 (1990).

¹⁵G. Kleinle, V. Penka, R. J. Behm, G. Ertl, and W. Moritz, *Phys. Rev. Lett.* **58**, 148 (1987).

¹⁶W. Reimer, V. Penka, M. Skottke, R. J. Behm, G. Ertl, and W. Moritz, *Surf. Sci.* **186**, 45 (1987).

¹⁷B. Voigtländer, S. Lehwald, and H. Ibach, *Surf. Sci.* **208**, 113 (1989).

¹⁸G. Parschau, B. Burg, and K. H. Rieder, *Surf. Sci. Lett.* **293**, L830 (1993).

¹⁹K. H. Rieder, *Surf. Rev. Lett.* **1**, 51 (1994).

²⁰P. Blaha, K.-H. Schwarz, P. Dufek, and R. Augustyn, WIEN95, Technical University of Vienna, 1995; P. Blaha, K.-H. Schwarz, P. Sorantin, and S. B. Trickey, *Comput. Phys. Commun.* **59**, 399 (1990).

²¹J. P. Perdew, J. A. Chevary, S. H. Vosko, K. A. Jackson, M. R. Pederson, D. J. Singh, and C. Fiolhais, *Phys. Rev. B* **46**, 6671 (1992); J. P. Perdew and Y. Wang, *ibid.* **45**, 13 244 (1992).

²²P. E. Blöchl, O. Jepsen, and O. K. Anderson, *Phys. Rev. B* **49**, 16 223 (1994).

²³G. Pacchioni and N. Rösch, *Acc. Chem. Res.* **28**, 390 (1995).

²⁴M. Tinkham, *Group Theory and Quantum Mechanics* (McGraw-Hill, New York, 1964).

²⁵U. Birkenheuer, Extensions to the WIEN95 code (Ref. 20), 1997.